HHS Public Access

Author manuscript

J Proteome Res. Author manuscript; available in PMC 2024 July 02.

Published in final edited form as:

J Proteome Res. 2024 June 07; 23(6): 1970–1982. doi:10.1021/acs.jproteome.3c00853.

Global Proteomic Analysis Reveals Alterations in Differentially Expressed Proteins Between Cardiopathic LMNA Mutations

Corey L. Anderson[1,†,*], **Kyle A. Brown**[2,†], **Ryan J. North**[1], **Janay K. Walters**[1], **Sara T. Kaska**[1], **Mathew R. Wolff**[1], **Timothy J. Kamp**[1], **Ying Ge**[2], **Lee L. Eckhardt**[1,*]

[1]Department of Medicine, Division of Cardiovascular Medicine, University of Wisconsin-Madison, Madison, WI 53705

[2]Department of Chemistry, University of Wisconsin-Madison, Madison, WI 53705

Abstract

Lamin A/C (LMNA) is an important component of the nuclear lamina. Mutations cause arrhythmia, heart failure, and sudden cardiac death. While LMNA-associated cardiomyopathy typically has an aggressive course that responds poorly to conventional heart failure therapies, there is variability in severity and age of penetrance between and even within specific mutations, which is poorly understood at the cellular level. Further, this heterogeneity has not previously been captured to mimic the heterozygous state nor have the hundreds of clinical LMNA mutations been represented. Herein, we have over-expressed cardiopathic LMNA variants in HEK cells and utilized state-of-the-art quantitative proteomics to compare the global proteomic profiles of 1) aggregating Q353K alone, 2) Q353K co-expressed with WT, 3) aggregating N195K co-expressed with WT and 4) non-aggregating E317K co-expressed with WT to help capture some of the heterogeneity between mutations. We analyzed each dataset to obtain the differentially expressed proteins (DEPs) and applied gene ontology (GO) and KEGG pathway analyses. We found a range of 162 to 324 DEPs from over 6000 total protein IDs with differences in GO terms, KEGG pathways and DEPs important in cardiac function further highlighting the complexity of cardiac

*Correspondence: clander2@wisc.edu.
†These authors contributed equally to this work.

Disclosures

The patient-specific LMNA N195K iPS cells used in this study are from co-author Dr. Matthew R. Wolff who is also founder of Table Bluff Life Sciences LLC. Dr. Timothy J. Kamp was a consultant for Fujifilm CDI, Inc.

Supporting Information

This article contains supporting information.

Figure S1. Properties of lamin mutations.
Figure S2. Protein abundance correlation plots.
Figure S3 and S4. WebGestalt GO term and KEGG Pathways analyses.
Figure S5. List of DEPs important for cardiac function.
Figure S6. Cardiac relevant DEPs.
Figure S7. Validation immunoblots.
Figure S8. LC-MS/MS analysis parameters.
Table S1. Data for functional assays (XLSX)
Table S2. DEPs for Q353K vs WT (XLSX)
Table S3. Data for GO analysis (XLXS)
Table S4. Data for KEGG analysis (XLSX)
Table S5. DEPs for WT/Q353K vs WT (XLSX)
Table S6. DEPs for WT/E317K vs WT (XLSX)
Table S7. DEPs for WT/N195K vs WT (XLSX)

laminopathies. Pathways disrupted by LMNA mutations were validated with redox, autophagy and apoptosis functional assays in both HEK 293 cells and in induced pluripotent stem cell derived cardiomyocytes (iPSC-CMs) for LMNA N195K. These proteomic profiles expand our repertoire for mutation-specific downstream cellular effects that may become useful as druggable targets for personalized medicine approach for cardiac laminopathies.

Keywords

lamin; genetic disease; cardiomyopathy; proteomics; protein aggregation

Introduction

Lamin A/C, encoded by LMNA, is an intermediate filament protein that forms the nuclear lamina with a myriad of functions in nuclear membrane shape and stability, chromatin organization, and transcriptional regulation among others[1]. Mutations in *LMNA* cause several clinical phenotypes including lipodystrophy, progeria, muscular dystrophy and cardiomyopathy[2]. The cardiac disease phenotype is a devastating disease dominated by lethal ventricular arrhythmias and left ventricular failure often necessitating transplant or precipitating death[3–7]. While several structural and/or transcriptional pathophysiologic mechanisms have been described[8], understanding of the arrhythmogenic and myopathic cellular pathogenesis remains limited, mainly due to the broad clinical phenotypic variability between families, the extensive number and types (missense, deletion, frame shift) of *LMNA* mutations and relatively small number of characterized laminopathy models[9,10]. Consequently, promising therapeutics have not translated to wide-spread clinical use and as of today no disease modifying therapy is available for patients with cardiac laminopathy[11,12].

To address LMNA mutation genotype-phenotype correlations, we previously created a library of 178 *LMNA* mutations associated with phenotypes of skeletal muscular dystrophy, cardiac disease, premature aging and lipodystrophy spanning the five structural domains of the lamin A protein (4 coiled-coil domains (CCD)[13] and C-terminal immunoglobulin-like domain (IgD))[14] (Fig. 1). We quantified lamin aggregation and protein misfolding, finding most cardiomypathic *LMNA* variants formed aggregates, but ~48% did not and many variants did not cause significant misfolding[15]. This systematic study revealed that even within a single clinical phenotype (cardiomyopathy), a high degree of cellular phenotypic variability exists. Further, we broaden the proteomic data beyond current restricted reports that are unlikely to be physiologically representative of all cardiac laminopathies.

Much of the “omics” level understanding of laminopathies come from $lmna^{KO}$ or $lmna^{H222P/H222P}$ mouse models[16,17]. These do not model the autosomal dominant nature of cardiac laminopathies nor the different aggregation propensities between mutants[15,18]. We suggest that cardiac laminopathy models which express both WT and mutant, include some aggregation-prone mutations, and include non-aggregating mutations will reveal more accurate cellular phenotypes and reveal new pathogenic mechanisms to therapeutically target.

We broaden the understanding of inter-disease phenotypic variability here by characterizing the global proteomic changes from heterozygous overexpression (mutant and WT) of a non-aggregating (E317K)[19,20] and two aggregating lamin A mutations (N195K and Q353K)[4,21,22]. We discovered that there was very little overlap in differentially expressed proteins (DEPs) between any of the mutations; many of which play important roles in cardiac function. Our global proteomic analysis also revealed several new cellular processes that are disrupted (e.g., ribosome and translation) and rediscovered several that have already been reported (i.e., autophagy[11], apoptosis[23], reductive stress[24,25]. The latter of which were validated using N195K patient induced pluripotent stem cell-derived cardiomyocyte cells (iPSC-CMs), demonstrating that cellular expression models identify disease pathways that can be new therapeutic targets[26].

Materials & Methods

Plasmids

All constructs were generated using a pcDNA3-GFP lamin N195K template from Addgene (#32708), which was mutated back to WT to use as a template for mutagenesis using the QuikChange II XL kit (Agilent) to generate the Q353K and E317K mutations as previously reported[15].

HEK 293 cell culture and transfection

HEK 293 cells (ATCC) were maintained in Dulbecco's Modified Eagle Medium (DMEM) containing 1 g/L glucose, 1 mM sodium pyruvate, 4 mM L- glutamine, and 10% FBS. HEK 293 cells of similar confluence (~90%) were transiently transfected with Lipofectamine 2000 (Invitrogen) using a DNA/lipofectamine ration of 1:3 same as previously reported for comparisons[15]. Transfected cells were grown at 37 °C for 24 h before imaging or MS preparations. All cells were maintained in a humidified incubator at 37 °C and 5% CO_2.

Immunoblot analysis

HEK 293 cells over-expressing each mutation were lysed 24 h after transfection and iPSC-CMs were lysed after day 30 from the start of differentiation (beating started ~day 10) with NP40 buffer containing Halt protease inhibitor (ThermoFisher). The soluble fraction was collected after a 10 min spin at 16,000 × *g*, run on SDS-PAGE and analyzed by immunoblot as previously described[15]. The antibodies and dilutions used for the Western blots were anti-GFP-HRP at 1:1000 (Santa Cruz), anti β-actin-HRP at 1:2000 (Santa Cruz), rabbit anti-SCO1 at 1:2000 (Proteintech) and donkey-anti-rabbit-HRP at 1:7500 (ThermoFisher).

iPSC culture and cardiomyocyte differentiation

iPS cells (normal volunteer DF19-9-11T.H cells from WiCell Stem Bank and patient N195K iPSCs) were maintained on Matrigel-coated plates using StemFlex media (ThermoFisher) before differentiating. iPSC-CMs were maintained on Matrigel-coated 6-well plates in RPMI +B27 with insulin (ThermoFisher) until imaging and functional assay experiments. All cells were maintained in a humidified incubator at 37 °C and 5% CO_2.

For cardiomyocyte differentiation, 19-9-11 (control) and patient N195K iPSCs were differentiated as previously described[15]. In brief, iPSCs maintained on StemFlex/ Matrigel were dissociated into single cells and seeded onto Matrigel-coated six-well plates. Cells were cultured for ~5 days in StemFlex medium until they reached 100% confluence. The differentiation (Day 0) started with changing the medium to RPMI + B27 supplement without insulin and 6 μM CHIR99021 (Tocris Bioscience). After 24 h (Day 1), the medium was changed to RPMI +B27 without insulin. After 48 h (Day 3), media was changed to RPMI +B27 without insulin containing 5 μM IWP2 (Tocris Bioscience). After 48 h (Day 5), the medium was changed to RPMI +B27 without insulin and then from day 7 and on maintained in RPMI +B27 with insulin. The differentiated cells (beating observed ~Day 10) were maintained with medium changes until Day 15 and then cryostored. Differentiated iPSC-CMs were purified by thawing and selecting in lactate medium (RPMI without glucose, B27 supplement, and 5 mM Sodium DL-lactate) for 10 days. iPSC-CMs were then maintained in RPMI +B27 until imaging or lysis post Day 30.

These studies of iPSCs were approved by the University of Wisconsin review board and abide by the Declaration of Helsinki principles.

Lamin A imaging and analysis

For HEK 293 cells, 24 h post transfection, live cells were imaged at 20× or 40× magnification using an EVOS FL Imaging System (ThermoFisher) that detected GFP tag fluorescence. The percentage of cells with lamin A aggregates were obtained by counting ≥100 cells from different fields of view averaged over at least three transfections. All images analyzed were blinded except for WT to test the quality of the transfected cells (i.e., no cytotoxicity and normal WT-like levels). Results of these were then compared to previously reported results of HEK 293 cells transfected with only lamin A mutant constructs[15]. The mean +/− standard deviation of at least three biological replicates was calculated and one-way ANOVA with Tukey post hoc test was used to determine statistical differences between variants and WT ($p < 0.05$).

For iPSC-CMs, lactate purified iPSC-CMs (20 days post CHIR treatment) were plated on gelatin-coated coverslips for two days, washed 1× with PBS and permeabilized in P-solution (3% dextran and 12.5 μg/ml digitonin in PBS) for 6 min. P-solution was washed out once with PBS and then fixed with 90% cold methanol for 5 min. Cells were then washed 2× with PBS and blocked in B-solution (5% goat serum and 0.3% Triton X-100 in PBS) for 30-min. 1:800 mouse anti-alpha-actinin (Sigma) and 1:500 rabbit anti-lamin A/C (Thermo Fisher) primary antibodies were added overnight at 4 °C, washed 3× with PBS, and then incubated with 1:1000 donkey anti-mouse Alexa Fluor 555 (RFP) and 1:2000 goat anti-rabbit Alexa Fluor 680 (Cy5) secondary antibodies (Thermo Fisher) in B-solution for 30 min in the dark. iPSC-CMs were then washed 3× with PBS and coverslips sealed with Prolong antifade mountant (Thermo Fisher) before imaging on a Leica Microsystems SP8 confocal microscope. For nuclear shape measurements, iPSC-CM nuclei were stained with DAPI and Image J used to analyze nuclear area, nuclear aspect ratio (major axis/minor axis) and nuclear circularity (4π(area/perimeter^2). The mean +/− standard deviation from 100 nuclei was calculated and students t-test was used to determine statistical differences

between variants and WT ($p < 0.05$). Figures and statistical analyses were done in GraphPad Prism 10.

Plate reader functional assays

HEK 293 cells were grown to ~90% confluence in 48 well plates and equal amounts of WT and mutant plasmids were transiently transfected as described above and assayed 24 h later. For iPSC-CMs, 10,000 lactate purified CMs were plated on Matrigel coated 48 well plates and maintained for at least two days in RPMI +B27 media. The day of the assay, media was removed, and cells were resuspended in 100 μL of PBS and 100 μL of either ROS-Glo, Caspase-Glo or Autophagy HiBiT Reporter assay reagent (Promega, Madison, WI) according to manufacturer's instructions. For ROS-Glo, cells were first incubated in hydrogen peroxide for 4 h in RPMI +B27. 100 μL of the reagent/cell mix was then transferred to a white-coated 96well plate and luminescent measurements were recorded on a Promega Glo-Max plate reader. The mean +/− standard deviation was calculated for each sample and one-way ANOVA with Tukey post hoc test was used to determine statistical differences between variants and WT ($p < 0.05$). Figures and statistical analyses were done in GraphPad Prism 10.

LC-MS/MS

WT plasmid (3 μg) or mutant plasmid co-expressed with WT plasmid (1.5 μg each) was transfected into HEK 293 cells using 60mm dishes (n=4) as described above. After 24 h, cells were washed 2× with PBS, pelleted at 1000 × *g* for 5-min and lysed in 250 μL of solubilization buffer (0.5% photocleavable 4-hexylphenylazosulfonate (AZO from Sigma)[27,28] in 25 mM Tris-HCl pH 7.5). Cells were first boiled for 10 min, incubated for another 30 min at room temp and reduced with 10 mM TCEP. Cysteines were then alkylated with 20 mM chloroacetamide for 30-min and soluble fraction was then collected after a 5 min spin at 16,000 × *g*. Sample was then incubated overnight at 37 °C with ~1μg trypsin:50μg protein followed by 1 h of 302 nm UV light exposure to cleave the surfactant. Trifluoroacetic acid was then added to 0.1% to stop trypsinization and soluble material was then collected after a 5-min spin at 16,000 × *g*. Samples were then desalted using 100 μL C18 Ziptips (Pierce) according to manufacturer's instructions and then vacuum dried. Dried pellets were then stored at −80 °C and resuspended in 25 μL 1% formic acid in water the day of analysis.

About 300 ng of peptide was injected onto an Ion Optics column (25 cm × 75 μm, C18 1.6 μm) heated to 55 °C and separated using a gradient of 3–30% mobile phase B (0.2% formic acid in ACN) over 60 min followed by a 5-min gradient of 30–95% B using a flow rate of 300 nL/min. Eluting peptides were directly ionized via electrospray ionization (CaptiveSpray) using a capillary voltage of 1650 V, dry temp of 181 °C and dry gas of 3.0 L/min. MS1 and MS2 spectra were taken from 100 to 1700 m/z using a timsTOF Pro Q-TOF (Bruker Daltonics) operating in diaPASEF mode[29–31] with parameters shown in Fig. S8. The collision energy was ramped linearly as a function of the mobility from 59.0 eV at 1/K0 = 1.6 Vs cm−2 to 19.99 eV at 1/K0 = 0.6 Vs cm−2.

Data were processed using DIA-NN V18.1 software[29,32]. For database searches, a spectral library was created using the reviewed Homo Sapiens UniProt sequences (https://www.uniprot.org, June 29, 2022). Carbamidomethyl (C) as a fixed modification and oxidation (M) and protein N-terminal acetylation were set as variable modifications. 1 missed cleavage and 1 variable modification was allowed. The mass accuracy was set to 10 ppm. A 1% false discovery rate was used and match between runs was enabled. Otherwise, the DIA-NN parameters were not changed from their default values. Two-sample t-tests were performed in Perseus[33] with p-values adjusted using the Permutation-based FDR (0.05) method. Protein abundance correlation plots for WT vs WT/mutant samples (n=4) are shown in Fig. S2.

Bioinformatic enrichment analysis of DEPs

Volcano plots were constructed using the webtool VolcaNoseR2 (https://huygens.science.uva.nl/VolcaNoseR2)[34]. All proteins that met the p-value of 0.05 threshold were considered DEPs without a fold change threshold since our transfection efficiency was only ~50% and overexpression was only for 24 h. The WEB-based Gene SeT AnaLysis Toolkit (http://www.webgestalt.org)[35] was used for functional enrichment analysis of DEPs. The over-representation method was used to analyze the Gene Ontology functional database for nonredundant biological processes, cellular composition, and molecular function. The KEGG Orthology-Based Annotation System (KOBAS) web tool (http://kobas.cbi.pku.edu.cn/home.do) was used to analyze the KEGG pathways database[36]. The clustered heatmap was generated using the Heatmapper web tool (http://www.heatmapper.ca) using the average linkage clustering method and Euclidean distance measurement method[37].

Results

Co-expressing WT partially corrects mutant lamin A aggregation

In addition to nuclear blebbing, we previously observed that ~50% of cardiopathic LMNA mutations also form nuclear aggregates upon homozygous expression (mutant alone) in HEK 293 cells[15]. However, myopathic laminopathies have autosomal dominant inheritance so we performed the same aggregation assay here for a small subset of 10 mutations upon heterozygous expression (mutant and WT) for comparison (example western blots are shown in Fig. S1). As shown in Fig. 2, A and B, nuclear aggregation remains a common feature for cardiomyopathic disease (e.g., Q353K), but for some mutations, (e.g., N195K and D357A) nuclear aggregation is decreased by WT co-expression (see also Table S1 and Fig. S1). Furthermore, we show that Q353K acts in a dominant-negative manner by interacting with and inducing WT aggregation (Fig. 2A). These results show that WT LMNA influences mutant LMNA aggregation and demonstrates the importance of co-expression of WT with mutant to resolve the physiologic cellular phenotype.

Q353K lamin A exhibits different proteomic changes compared to co-expression with WT

We sought to quantitatively determine the global proteomic profile of an aggregating mutant (Q353K)[15,40], expressed alone compared to heterozygous expression with WT (Fig. 1). Proteins were extracted from HEK 293 cells expressing homomeric Q353K

lamin A or WT using a photocleavable anionic surfactant (Azo)[27,28] and digested with trypsin. The resulting peptides were sequenced using reversed-phase liquid chromatography coupled to tandem mass spectrometry (LC-MS/MS) using trapped ion mobility spectrometry (TIMS) quadrupole time-of-flight (QTOF) mass spectrometry analysis operated in parallel accumulation-serial fragmentation (PASEF) mode[41,42]. 5,337 proteins (Fig. 3A) of which 125 were down-regulated ($p_{adj} < 0.05$) and 25 were up-regulated ($p_{adj} < 0.05$) (Table S2) compared to WT lamin A. Protein abundances were high correlated (>0.88) between biological (n=4) and condition replicates (Fig. S2). This result gives us confidence that the observed DEPs are likely derived from biological perturbations rather than technical variations.

From this dataset of DEPs, we performed gene ontology (GO) of biological process, cellular component, and molecular function categories overrepresentation (Fig. S3 and Table S3) and a KEGG pathways analysis (Fig. S3 and Table S4) of the unique Entrez gene IDs shown in Table S2. We highlight the important cellular processes disrupted for down-regulated proteins in Fig. S3 such as autophagic mechanisms, AMPK signaling, RNA activity, and helicase activity, while up-regulated proteins were associated with chromosome organization, apoptosis, and ER stress (Fig. S4).

For comparison, we performed MS analysis of Q353K lamin A co-expressed with WT in HEK 293 cells and identified 6028 proteins (Fig. 3B) of which 128 were down-regulated ($p_{adj} < 0.05$) and 35 were up-regulated ($p_{adj} < 0.05$) (Table S5) compared to WT LMNA. From this dataset of DEPs, we performed the same GO (Fig. S3 and Table S3) and KEGG (Fig. S3 and Table S4) analyses and found similar cellular processes as that of homomeric Q353K. For example, down-regulated proteins were associated with autophagy and RNA processes (splicing and transport), while up-regulated proteins were associated with the spliceosome and proteolysis. Interestingly, the DEPs identified showed limited overlap (Fig. 3C) despite overlap of overall cellular processes.

Non-aggregating E317K lamin A disrupts different cellular processes than aggregating Q353K

We previously identified that ~50% of LMNA variants associated with cardiomyopathies do not demonstrate cellular aggregates including E317K (**Anderson 2021**).[15] Here, we performed quantitative global proteomics on non-aggregating E317K lamin A co-expressed with WT in HEK 293 cells to compare with aggregating Q353K above. We identified 6028 proteins (Fig. 4A) of which 82 were down-regulated ($p_{adj} < 0.05$) and 117 were up-regulated ($p_{adj} < 0.05$) (Table S6) compared to WT LMNA. From this dataset of DEPs, we performed the same GO (Fig. S4 and Table S3) and KEGG (Fig. S4 and Table S4) analyses as described above. Here, the down-regulated proteins were most associated with disrupted cellular processes with up-regulated proteins showing no significant associations. Down-regulated proteins' GO Terms for E317K were associated with RNA catabolism, translation initiation, protein localization to ER, and ribosome constituents. KEGG pathway associations included the ribosome, purine metabolism, and several pathways (metabolic, mRNA surveillance, ErbB signaling, and NF-κB signaling). Interestingly, non-aggregating WT/E317K DEPs showed little overlap with aggregating WT/Q353K (Fig. 4C).

Aggregating N195K is more disruptive than Q353K and E317K.

We next investigated if the aggregating variant Q353K would behave similarly to another aggregating mutant N195K, despite that N195K was less aggregation-prone compared to Q353K in our previous study. Global quantitative proteomics of N195K lamin A co-expressed with WT in HEK 293 cells identified 6029 proteins (Fig. 4B) of which 151 were down-regulated ($p_{adj} < 0.05$) and 174 were up-regulated ($p_{adj} < 0.05$) (Table S7). From this dataset of DEPs, we performed the same GO (Fig. S4 and Table S3) and KEGG analyses (Fig. S4 and Table S4) and found many more changes in cellular processes than Q353K and E317K. For example, down-regulated proteins associated strongly with several ribosome functions and processes, RNA splicing, protein targeting and localization as well as metabolic and TNF signaling pathways, while up-regulated proteins associated with numerous processes and pathways including protein complex localization, mechanoreceptor differentiation, cell adhesion, as well as ATPase and motor activities. KEGG pathways include ribosome, protein processing in ER, tight junction, metabolic pathways, apoptosis, non-homologues end-joining and glutathione metabolism.

DEPs are enriched in cardiac function.

Overall, DEPs had surprisingly little overlap between mutations as shown in the Venn diagram in Fig. 4C and clustered heatmap in Fig. 4D despite some overlap in GO Terms and KEGG pathways, which is summarized in Fig. 5A. For example, all mutations disrupt RNA catabolism and the ribosome which has over two dozen associated proteins among the three mutations (Fig. 5B). DEPs also associate with different cellular phenotypes and downstream effects as seen between aggregating (e.g. Q353K) and non-aggregating (e.g. E317K) mutants. In general, aggregation causes more changes in processes related to protein and cellular homeostasis such autophagy, apoptosis, and ER stress response unlike the non-aggregating mutant. In contrast, non-aggregating E317K caused more changes in processes related to translation unlike aggregating mutants. Interestingly, WT/N195K, which only slightly aggregated in HEK cells and not observed in iPSC-CMs (Fig. 6D) had the largest number of DEPs and broadest impact altering the most processes. Finally, we observed upon over-expression in HEK cells that while all mutations impacted ROS, only those most aggregation prone impacted apoptosis and autophagy. These results help explain why genotype-phenotype correlations remain unclear for laminopathies. Perhaps a larger proteomic comparison of aggregating and non-aggregating mutations across a different region of lamin A/C might reveal more overlap between mutations.

Finally, a literature search revealed dozens of DEPs that have been reported to play an important role in cardiac (dys)function for each mutation listed in Fig. S5. To give just a few examples, FHL1 was down-regulated 35% in WT/Q353K and harbors mutations linked to Emery-Dreifuss muscular dystrophy (EDMD)[43] and hypertrophic cardiomyopathy (HCM)[44] (Fig. S6). This highlights the cellular phenotypic overlap as EDMD is the most common clinical skeletal muscle phenotype of laminopathies and ~80% of skeletal muscle mutations aggregate including the two shown in Fig. 2B (Y45C and R101P)[15]. ECSIT was down-regulated 50% in WT/E317K and leads to cardiac mitochondrial dysfunction when low levels are present in a mouse model (**Xu 2021**[45] (Fig. S6). Lastly, for WT/N195K, GAB1 was down-regulated 34%, which leads to DCM with mitochondrial damage and apoptosis

when deleted (**Zhao 2016**[46]. The alpha-actinin binding LDB3 was also down-regulated 24% and reported to cause pediatric dilated cardiomyopathy (DCM)[47] (Table S7). More of these examples are highlighted in Fig. S6, which reveal numerous potential responses that could have an impact on cardiac function either individually or cumulatively, which leads to cardiomyopathy.

Functional validation of MS results: increased apoptosis, reduced autophagy, and reductive stress

First, we performed some immunoblot validation of the proteomics results for the mitochondrial protein SCO1 (Synthesis of Cytochrome C Oxidase 1) involved in copper homeostasis and associated with cardiomyopathy[48], which was up-regulated in E317K and N195K (Fig. 4A,B and D). Immunoblot analysis of HEK 293 cells overexpressing E317K and N195K both showed an increase in expression compared to WT (Fig. S7) In contrast, ACTB (β-actin), which was not differentially regulated (Fig. 4A and B), showed similar expression levels to WT for both mutations (Fig. S7).

To validate some of the GO and KEGG results, we performed three different functional analyses. First, we studied apoptosis since KEGG analysis showed that it was dysregulated in Q353K and N195K (Fig. 5A). Using Caspase 3/7 activity, we found that all mutations, when overexpressed as homozygotes in HEK 293 cells show an increase in activity as well as Q353K co-expressed with WT (Fig. 6A, Table S1). Next, since many DEPs were mitochondrial, and KEGG analysis showed changes in metabolism (e.g., glutathione metabolism and ATPase activity) (Fig. 5A), we studied redox activity by measuring the reactive oxygen species hydrogen peroxide. Fig. 6B and Table S1 shows that all homozygous and heterozygous expressed mutations exhibit decreased ROS levels indicating reductive stress, which has been reported as a feature of laminopathies[25] and and potentially modulate for therapeutic benefit[49]. Last, our GO Term analysis demonstrated autophagy disruption for homozygous expression of Q353K. We performed an autophagic flux assay across all mutations and similarly found a small but statistically significant decrease in autophagy for Q353K when expressed alone (Fig. 6C and Table S1). This suggests that other mutations may also be a potential target for autophagy modulation, which has been demonstrated for the H222P mutation[50].

Next, we wanted to validate some of our proteomics results using iPSC-CMs. We generated iPSC-CMs from a patient harboring N195K[51] as well as from a normal volunteer (19-9-11) to serve as a control[52]. Immunofluorescence staining of lamin A/C and α-actinin of iPSC-CMs plated on a 30um, 15° chevron pattern[53] did not exhibit any nuclear aggregation or changes in sarcomere organization (Fig. 6D). This is consistent with our HEK 293 overexpression results that showed co-expression of WT with N195K significantly reduced lamin A aggregation (Fig. 2B). However, the patient iPSC-CMs had smaller nuclei and abnormal nuclear shape (Fig. 6E and Table S1), which is a hallmark of laminopathies. Next, we performed the same immunoblot validation for SCO1, and found the N195K patient iPSC-CMs showed an increase in expression compared to 19-9-11 control iPSC-CMs relative to β-actin expression (Fig. S7). Finally, we found that the N195K patient iPSC-CMs showed an increase in caspase activity (i.e., apoptosis) (Fig. 6F and Table S1) as well as

decreased levels of hydrogen peroxide (Fig. 6G), like our HEK 293 over-expression model. Together, these results suggest that HEK 293 over-expression is a relatively simple and useful model for laminopathy proteomics studies as well as some functional analyses.

Discussion

This study highlights that different *LMNA* mutations have multiple downstream effects and cellular phenotypic expressions with mutation-specific proteomic profiles that have overlapping effects on similar cellular processes. We hypothesized that a higher degree of convergence between mutations would be present. We also identified multiple knowledge gaps of specific downstream effects and our ability to resolve upstream modulators. Moreover, the relatively small number of characterized variants in the literature to date may have resulted in disease oversimplification and missed therapeutic targets for ameliorating cardiac laminopathies. Our study starts to unravel a number of these possible targets. Finally, we validate other targets that have been previously reported and therapeutically targeted, showing that this data-driven overexpression model approach is a valuable starting point.

DNA and RNA damage

DNA and RNA transcript damage has been recognized for several mutations with disruption of the nuclear lamina. For example, *LMNA* N195K mouse muscle fibers exhibit DNA damage comparable to *LMNA* KO mice, while damage to *lmna*$^{H222P/H222P}$ mice was less severe[54]. Our KEGG and GO Term analyses showed disruptions in DNA processes including non-homologous endjoining, the major DNA break repair pathway, for N195K. RNA processes were also disrupted including RNA catabolism for all mutations, mRNA surveillance for E317K and RNA splicing for Q353K and N195K. To highlight just one protein, the RNAPIII regulator MAF1, down-regulated 50% in Q353K, was shown to ameliorate cardiac hypertrophy through ERK1/2-signaling, which has been implicated and targeted for LMNA-cardiomyopathy[55,56]. Further, dysregulation of chromosome regulation is a pathological feature of laminopathies[57], which we observed with N195K.

Ribosomal Disruption

Perhaps the most strikingly disrupted processes we observed from our proteomics data is the ribosome. There were 16 ribosomal proteins (two are mitochondrial) and another 6 important in its biogenesis that were down-regulated in one or more of the mutations (e.g., RPLP1, RPL15, RPL27A by 30%). A systematic knockdown analysis of ribosomal proteins in human cells revealed altered expression of genes involved in cellular metabolism, signal transduction and development[58]. This is interesting as alternative fate protein synthesis has also been reported for isolated *LMNA* mutations[59]. Numerous ribosomopathies have been described as well and ribosomal protein deficiencies exhibit cardiomyopathy in a Drosophila model, so this might be an underappreciated laminopathic mechanism to target[60].

Autophagy and apoptosis

We found DEPs involved in proteostasis and cellular homeostasis (i.e., ER stress, ubiquitin-mediated proteolysis, autophagy, apoptosis) mostly for the aggregation prone Q353K and N195K LMNA mutations (Fig. S7B) but also for E317K where the ubiquitous E2 ligase

(UBE2I) was down-regulated ~30%. UBE2I is involved in SUMOylation (small ubiquitin like modifiers) that regulates lamin degradation which is lost in cardiac laminopathies[61]. A deletion LMNA mutation associated with DCM has also been shown to cause ER stress with abnormal Ca^{2+} handling so this might be a common mechanism for a subset of mutations[62]. Dysfunctional autophagy has long been recognized with laminopathies but may not be universally strong for all mutations. We found that the important autophagy protein ULK-1 is down-regulated by ~40% in Q353K which also had reduced autophagic flux. However, this change was small and only seen with homozygous Q353K expression and so it is unclear if there is a biologically meaningful effect. Further validation studies in iPSC-cardiomyocytes with heterologous expression of Q353K would address this and if so, autophagy reactivation strategies might benefit select mutations like Q353K (and reported H222P)[50] but may not be a feature for all cardiac laminopathies. Increased apoptosis has also been implicated in a E82K mouse model[23] and several iPSC-CM models (e.g., R377H) of laminopathic DCM[63]. Similarly, our proteomic analysis revealed up-regulation of several apoptotic proteins in N195K and Q353K but not in E317K again suggesting subsets of apoptosis prone mutations.

Mitochondrial dysfunction and redox homeostasis

Mitochondrial dysfunction and redox homeostasis (i.e., oxidative and reductive stress) are thought to be features of laminopathies[25,64–67]. For mitochondrial function, our proteomic data revealed dysregulation of several important proteins for all mutations including: 1) the mitochondrial ATPase subunits MT-ATP8 and ATP5MF are down-regulated ~30% in N195K, 2) the membrane transporter TOMM22 and complex 1 subunit NDUFS8 are down-regulated ~25% in Q353K, 3) ECSIT, an assembly factor for mitochondrial complex 1 and cardiac function, was down-regulated ~50% in E317K and deficiency impairs oxidative phosphorylation (OXPHOS) and ATP production[45]). For oxidative stress, the superoxide dismutase (SOD2), an important mitochondrial protein that scavenges ROS and an indicator of DCM[68] outcomes is up-regulated 1.5× in N195K. In contrast, LANCL1, which catalyzes conjugation of glutathione to substrates in the oxidative stress response is down-regulate 50% in N195K. The protease LONP2, an important component of mitochondrial quality control, is down-regulated by ~50% in Q353K and deficiency negatively affects mitochondrial gene expression, OXPHOS and consequently protection against oxidative stress[69]. Finally, peroxiredoxin (PRDX6), which is implicated in cardiovascular disease[70], was one of only two down-regulated DEPs identified for all three mutations. This result is surprising since PRDX6 eliminates peroxide and other peroxide eliminating enzymes like catalase and glutathione peroxidases showed no changes. However, redox regulation is complex with dozens of enzymes involved in peroxide formation which may offset the PRDX6 changes, which were a small 15–25% reduction across all three mutations and may not be a significant factor. All mutations studied were under reductive stress in our functional analysis suggesting common redox mechanisms that may offer therapeutic targets for modulation[24,49].

Signaling pathways

Finally, disruption in various signaling pathways is an important feature of cardiac laminopathies and the basis for some lamin-specific treatments. Our proteomic dataset

revealed changes in signaling pathways such as NFκB, a mechanical stress responsive transcription factor, is dysregulated in E317K in our dataset as well as HEK 293 laminopathy model of I373V[71], lmna^{KO} mouse model[72], lmna$^{H222P/H222P}$ mouse model[73], DCM-linked D300N mouse model[74] and premature aging mouse model[75]. Another example is AMPK, a master regulator of cellular energy metabolism, which was dysregulated in our Q353K dataset as well as in human muscle tissue for the G449V-linked laminopathy[76]. These processes and pathways are not mutually exclusive with interplay between most[77]. For example, mutations that aggregate or perturb ER homeostasis could trigger proteasomal, apoptotic, and/or autophagic pathways for which there is crosstalk[78]. Scaffolding proteins are another example that can have numerous effects including contractility, signaling and apoptosis when dysfunctional. Indeed, we found two scaffolding proteins GAB1 and BNIP2 to be down-regulated 34% and 53%, respectively in N195K. The former leads to DCM in a knockout mouse with mitochondrial dysfunction and CM apoptosis[46], while the latter shows reduced contractile force in depleted iPSC-CMs[79]. Further, the sarcomere protein FHL1 implicated in several myopathies including EDMD with cardiac disease was down-regulated 35% in Q353K[43]. These examples highlight just some of the dozens of dysregulated proteins important in cardiac function we found from our relatively small proteomic analysis.

Limitations

We recognize that there are some limitations in the overexpression model used. First, differentiated cells express lamin A/C but nuclear proteomes can differ[80] and therefore the effect of LMNA mutations may be different in cardiac cells. Second, HEK 293 cells may not reflect ion channels and Ca^{2+} handling proteins as cardiac cells. Ca^{2+} mishandling is a prominent feature in heart failure for laminopathies[81–83] and intracellular Ca^{2+} dysregulation is a central component for both atrial fibrillation, ventricular tachycardia and ventricular fibrillation[66,84,85]. Thus, the identification of upstream modulators of key Ca^{2+} handling proteins remain important targets for cardiac laminopathy disease modulation. We are actively working on resolving this with additional studies in iPSC-cardiomyocyte models. Fourth, variability in lamin A expression levels between mutations may introduce some noise unrelated to their pathogenesis. However, as shown in the volcano plots, WT/N195K and Q353K alone had only slight 1.1- and 1.3-fold increases in lamin A levels compared to WT, respectively. Finally, the short expression time in HEK 293 cells may underrepresent chronic changes such as autophagy, which was decreased with the most aggregation prone condition (Q353K alone) but may present over a longer time course. However, this model identifies important cardiac relevant DEPs that may provide new clues to the downstream temporal changes seen early in the disease process and may represent early drug targets. These early markers may also have identified underappreciated mechanisms including ribosome and mitochondrial dysfunction that may ultimately contribute to the downstream effects seen in heart failure. Nevertheless, the results reported herein serve as a good starting point for identifying new laminopathic mechanisms to validate and potentially test in an isogenic iPSC-CM laminopathy model (e.g., reductive stress, apoptosis and autophagy identified herein for N195K).

Conclusions

In this study we identify LMNA mutation-specific proteomic profiles that shared similar downstream effects including DNA/RNA damage, ribosomal disruption, faulty apoptosis/autophagy, mitochondrial damage and signaling disruption. Uniquely, while the downstream pathways were similar, each mutation had DEPs that were mutation specific and modified upon co-expression with WT. We reaffirmed some known cellular downstream effects of LMNA mutations while identifying strong early markers that have not previously been recognized. Importantly, our proteomic profiles were validated with functional studies and in patient-specific iPSC-CMs to further strengthen our findings. Overall, this study expands our repertoire for mutation-specific downstream cellular effects that may become useful as druggable targets for personalized medicine approaches for cardiac laminopathies.

Supplementary Material

Refer to Web version on PubMed Central for supplementary material.

Funding and additional information

This study was supported by NIH/NHLBI F32 HL162374 (KAB), R01 HL163987 (LLE), R01 HL163987 (LLE), and NHLBI R01 HL139738 (LLE). The content is solely the responsibility of the authors and does not necessarily represent the official views of the National Institute of Health. This study was funded in part by the Gary and Marie Weiner Professor of Cardiovascular Medicine Research (LLE). Funding from the Wisconsin Partnership Program supported the generation of the LMNA N195K iPS cell line (TJK). Y.G. would like to acknowledge support from the NIH R01 HL109810 and S10OD018475 (for the acquisition of the ultra-high resolution mass spectrometer).

Data Availability

The mass spectrometry proteomics data has been deposited to the ProteomeXchange Consortium[38] via the PRIDE[39] partner repository with the dataset identifier PXD045092. Plasmids and/or iPS cells are available from the corresponding author upon reasonable request.

References

(1). Dittmer TA; Misteli T The Lamin Protein Family. Genome Biol 2011, 12 (5), 222. 10.1186/gb-2011-12-5-222. [PubMed: 21639948]

(2). Captur G; Arbustini E; Bonne G; Syrris P; Mills K; Wahbi K; Mohiddin SA; McKenna WJ; Pettit S; Ho CY; Muchir A; Gissen P; Elliott PM; Moon JC Lamin and the Heart. Heart 2018, 104 (6), 468. 10.1136/heartjnl-2017-312338. [PubMed: 29175975]

(3). Gigli M; Merlo M; Graw SL; Barbati G; Rowland TJ; Slavov DB; Stolfo D; Haywood ME; Ferro MD; Altinier A; Ramani F; Brun F; Cocciolo A; Puggia I; Morea G; McKenna WJ; Rosa FGL; Taylor MRG; Sinagra G; Mestroni L Genetic Risk of Arrhythmic Phenotypes in Patients With Dilated Cardiomyopathy. J. Am. Coll. Cardiol. 2019, 74 (11), 1480–1490. 10.1016/j.jacc.2019.06.072. [PubMed: 31514951]

(4). Fatkin D; MacRae C; Sasaki T; Wolff MR; Porcu M; Frenneaux M; Atherton J; Vidaillet HJ; Spudich S; Girolami UD; Seidman JG; Muntoni F; Müehle G; Johnson W; McDonough B; Seidman CE Missense Mutations in the Rod Domain of the Lamin A/C Gene as Causes of Dilated Cardiomyopathy and Conduction-System Disease. New Engl J Med 1999, 341 (23), 1715–1724. 10.1056/nejm199912023412302. [PubMed: 10580070]

(5). Hasselberg NE; Haland TF; Saberniak J; Brekke PH; Berge KE; Leren TP; Edvardsen T; Haugaa KH Lamin A/C Cardiomyopathy: Young Onset, High Penetrance, and Frequent Need for Heart Transplantation. Eur. Hear. J. 2018, 39 (10), 853–860. 10.1093/eurheartj/ehx596.

(6). Taylor MRG; Fain PR; Sinagra G; Robinson ML; Robertson AD; Carniel E; Lenarda AD; Bohlmeyer TJ; Ferguson DA; Brodsky GL; Boucek MM; Lascor J; Moss AC; Li W-LP; Stetler GL; Muntoni F; Bristow MR; Mestroni L; Group FDCRR Natural History of Dilated Cardiomyopathy Due to Lamin A/C Gene Mutations. J. Am. Coll. Cardiol. 2003, 41 (5), 771–780. 10.1016/s0735-1097(02)02954-6. [PubMed: 12628721]

(7). Captur G; Arbustini E; Syrris P; Radenkovic D; O'Brien B; Mckenna WJ; Moon JC Lamin Mutation Location Predicts Cardiac Phenotype Severity: Combined Analysis of the Published Literature. Open Hear 2018, 5 (2), e000915. 10.1136/openhrt-2018-000915.

(8). Osmanagic-Myers S; Foisner R The Structural and Gene Expression Hypotheses in Laminopathic Diseases—Not so Different after All. Mol Biol Cell 2019, 30 (15), 1786–1790. 10.1091/mbc.e18-10-0672. [PubMed: 31306095]

(9). Hoorntje ET; Bollen IA; Barge-Schaapveld DQ; Tienen F. H. van; Meerman G. J. te; Jansweijer JA; Essen A. J. van; Volders PG; Constantinescu AA; Akker P. C. van den; Spaendonck-Zwarts K. Y. van; Oldenburg RA; Marcelis CL; Smagt J. J. van der; Hennekam EA; Vink A; Bootsma M; Aten E; Wilde AA; Wijngaard A. van den; Broers JL; Jongbloed JD; Velden J. van der; Berg M. P. van den; Tintelen J. P. van. Lamin A/C-Related Cardiac Disease. Circ.: Cardiovasc. Genet. 2017, 10 (4), e001631. 10.1161/circgenetics.116.001631. [PubMed: 28790152]

(10). Yang J; Argenziano MA; Angulo MB; Bertalovitz A; Beidokhti MN; McDonald TV Phenotypic Variability in IPSC-Induced Cardiomyocytes and Cardiac Fibroblasts Carrying Diverse LMNA Mutations. Front. Physiol. 2021, 12, 778982. 10.3389/fphys.2021.778982. [PubMed: 34975533]

(11). Choi JC; Muchir A; Wu W; Iwata S; Homma S; Morrow JP; Worman HJ Temsirolimus Activates Autophagy and Ameliorates Cardiomyopathy Caused by Lamin A/C Gene Mutation. Sci. Transl. Med. 2012, 4 (144), 144ra102. 10.1126/scitranslmed.3003875.

(12). DuBose AJ; Lichtenstein ST; Petrash NM; Erdos MR; Gordon LB; Collins FS Everolimus Rescues Multiple Cellular Defects in Laminopathy-Patient Fibroblasts. Proc. Natl. Acad. Sci. 2018, 115 (16), 4206–4211. 10.1073/pnas.1802811115. [PubMed: 29581305]

(13). Ahn J; Jo I; Kang S; Hong S; Kim S; Jeong S; Kim Y-H; Park B-J; Ha N-C Structural Basis for Lamin Assembly at the Molecular Level. Nat Commun 2019, 10 (1), 3757. 10.1038/s41467-019-11684-x. [PubMed: 31434876]

(14). Dhe-Paganon S; Werner ED; Chi Y-I; Shoelson SE Structure of the Globular Tail of Nuclear Lamin. J Biol Chem 2002, 277 (20), 17381–17384. 10.1074/jbc.c200038200. [PubMed: 11901143]

(15). Anderson CL; Langer ER; Routes TC; McWilliams SF; Bereslavskyy I; Kamp TJ; Eckhardt LL Most Myopathic Lamin Variants Aggregate: A Functional Genomics Approach for Assessing Variants of Uncertain Significance. npj Genom. Med. 2021, 6 (1), 103. 10.1038/s41525-021-00265-x. [PubMed: 34862408]

(16). Arimura T; Helbling-Leclerc A; Massart C; Varnous S; Niel F; Lacène E; Fromes Y; Toussaint M; Mura A-M; Keller DI; Amthor H; Isnard R; Malissen M; Schwartz K; Bonne G Mouse Model Carrying H222P- Lmna Mutation Develops Muscular Dystrophy and Dilated Cardiomyopathy Similar to Human Striated Muscle Laminopathies. Hum. Mol. Genet. 2005, 14 (1), 155–169. 10.1093/hmg/ddi017. [PubMed: 15548545]

(17). Gerbino A; Procino G; Svelto M; Carmosino M Role of Lamin A/C Gene Mutations in the Signaling Defects Leading to Cardiomyopathies. Front Physiol 2018, 9, 1356. 10.3389/fphys.2018.01356. [PubMed: 30319452]

(18). Piekarowicz K; Machowska M; Dratkiewicz E; Lorek D; Madej-Pilarczyk A; Rzepecki R The Effect of the Lamin A and Its Mutants on Nuclear Structure, Cell Proliferation, Protein Stability, and Mobility in Embryonic Cells. Chromosoma 2017, 126 (4), 501–517. 10.1007/s00412-016-0610-9. [PubMed: 27534416]

(19). Arbustini E; Pilotto A; Repetto A; Grasso M; Negri A; Diegoli M; Campana C; Scelsi L; Baldini E; Gavazzi A; Tavazzi L Autosomal Dominant Dilated Cardiomyopathy with Atrioventricular Block: A Lamin A/C Defect-Related Disease. J. Am. Coll. Cardiol. 2002, 39 (6), 981–990. 10.1016/s0735-1097(02)01724-2. [PubMed: 11897440]

(20). Ferradini V; Cosma J; Romeo F; Masi CD; Murdocca M; Spitalieri P; Mannucci S; Parlapiano G; Lorenzo FD; Martino A; Fedele F; Calò L; Novelli G; Sangiuolo F; Mango R Clinical Features of LMNA-Related Cardiomyopathy in 18 Patients and Characterization of Two Novel Variants. J. Clin. Med. 2021, 10 (21), 5075. 10.3390/jcm10215075. [PubMed: 34768595]

(21). Mounkes LC; Kozlov SV; Rottman JN; Stewart CL Expression of an LMNA-N195K Variant of A-Type Lamins Results in Cardiac Conduction Defects and Death in Mice. Hum. Mol. Genet. 2005, 14 (15), 2167–2180. 10.1093/hmg/ddi221. [PubMed: 15972724]

(22). Gupta P; Bilinska ZT; Sylvius N; Boudreau E; Veinot JP; Labib S; Bolongo PM; Hamza A; Jackson T; Ploski R; Walski M; Grzybowski J; Walczak E; Religa G; Fidzianska A; Tesson F Genetic and Ultrastructural Studies in Dilated Cardiomyopathy Patients: A Large Deletion in the Lamin A/C Gene Is Associated with Cardiomyocyte Nuclear Envelope Disruption. Basic Res. Cardiol. 2010, 105 (3), 365–377. 10.1007/s00395-010-0085-4. [PubMed: 20127487]

(23). Lu D; Lian H; Zhang X; Shao H; Huang L; Qin C; Zhang L LMNA E82K Mutation Activates FAS and Mitochondrial Pathways of Apoptosis in Heart Tissue Specific Transgenic Mice. PLoS ONE 2010, 5 (12), e15167. 10.1371/journal.pone.0015167. [PubMed: 21151901]

(24). Coombs GS; Rios-Monterrosa JL; Lai S; Dai Q; Goll AC; Ketterer MR; Valdes MF; Uche N; Benjamin IJ; Wallrath LL Modulation of Muscle Redox and Protein Aggregation Rescues Lethality Caused by Mutant Lamins. Redox Biol. 2021, 48, 102196. 10.1016/j.redox.2021.102196. [PubMed: 34872044]

(25). Dialynas G; Shrestha OK; Ponce JM; Zwerger M; Thiemann DA; Young GH; Moore SA; Yu L; Lammerding J; Wallrath LL Myopathic Lamin Mutations Cause Reductive Stress and Activate the Nrf2/Keap-1 Pathway. PLoS Genet. 2015, 11 (5), e1005231. 10.1371/journal.pgen.1005231. [PubMed: 25996830]

(26). Lee J; Termglinchan V; Diecke S; Itzhaki I; Lam CK; Garg P; Lau E; Greenhaw M; Seeger T; Wu H; Zhang JZ; Chen X; Gil IP; Ameen M; Sallam K; Rhee J-W; Churko JM; Chaudhary R; Chour T; Wang PJ; Snyder MP; Chang HY; Karakikes I; Wu JC Activation of PDGF Pathway Links LMNA Mutation to Dilated Cardiomyopathy. Nature 2019, 572 (7769), 335–340. 10.1038/s41586-019-1406-x. [PubMed: 31316208]

(27). Brown KA; Chen B; Guardado-Alvarez TM; Lin Z; Hwang L; Ayaz-Guner S; Jin S; Ge Y A Photocleavable Surfactant for Top-down Proteomics. Nat. Methods 2019, 16 (5), 417–420. 10.1038/s41592-019-0391-1. [PubMed: 30988469]

(28). Brown KA; Tucholski T; Eken C; Knott S; Zhu Y; Jin S; Ge Y High-Throughput Proteomics Enabled by a Photocleavable Surfactant. Angew. Chem. Int. Ed. 2020, 59 (22), 8406–8410. 10.1002/anie.201915374.

(29). Demichev V; Szyrwiel L; Yu F; Teo GC; Rosenberger G; Niewienda A; Ludwig D; Decker J; Kaspar-Schoenefeld S; Lilley KS; Mülleder M; Nesvizhskii AI; Ralser M Dia-PASEF Data Analysis Using FragPipe and DIA-NN for Deep Proteomics of Low Sample Amounts. Nat. Commun. 2022, 13 (1), 3944. 10.1038/s41467-022-31492-0. [PubMed: 35803928]

(30). Meier F; Brunner A-D; Koch S; Koch H; Lubeck M; Krause M; Goedecke N; Decker J; Kosinski T; Park MA; Bache N; Hoerning O; Cox J; Räther O; Mann M Online Parallel Accumulation–Serial Fragmentation (PASEF) with a Novel Trapped Ion Mobility Mass Spectrometer*. Mol. Cell. Proteom. 2018, 17 (12), i–2545. 10.1074/mcp.tir118.000900.

(31). Meier F; Brunner A-D; Frank M; Ha A; Bludau I; Voytik E; Kaspar-Schoenefeld S; Lubeck M; Raether O; Bache N; Aebersold R; Collins BC; Röst HL; Mann M DiaPASEF: Parallel Accumulation–Serial Fragmentation Combined with Data-Independent Acquisition. Nat. Methods 2020, 17 (12), 1229–1236. 10.1038/s41592-020-00998-0. [PubMed: 33257825]

(32). Demichev V; Messner CB; Vernardis SI; Lilley KS; Ralser M DIA-NN: Neural Networks and Interference Correction Enable Deep Proteome Coverage in High Throughput. Nat. Methods 2020, 17 (1), 41–44. 10.1038/s41592-019-0638-x. [PubMed: 31768060]

(33). Tyanova S; Temu T; Sinitcyn P; Carlson A; Hein MY; Geiger T; Mann M; Cox J The Perseus Computational Platform for Comprehensive Analysis of (Prote)Omics Data. Nat. Methods 2016, 13 (9), 731–740. 10.1038/nmeth.3901. [PubMed: 27348712]

(34). Goedhart J; Luijsterburg MS VolcaNoseR Is a Web App for Creating, Exploring, Labeling and Sharing Volcano Plots. Sci. Rep. 2020, 10 (1), 20560. 10.1038/s41598-020-76603-3. [PubMed: 33239692]

(35). Liao Y; Wang J; Jaehnig EJ; Shi Z; Zhang B WebGestalt 2019: Gene Set Analysis Toolkit with Revamped UIs and APIs. Nucleic Acids Res. 2019, 47 (W1), W199–W205. 10.1093/nar/gkz401. [PubMed: 31114916]

(36). Bu D; Luo H; Huo P; Wang Z; Zhang S; He Z; Wu Y; Zhao L; Liu J; Guo J; Fang S; Cao W; Yi L; Zhao Y; Kong L KOBAS-i: Intelligent Prioritization and Exploratory Visualization of Biological Functions for Gene Enrichment Analysis. Nucleic Acids Res. 2021, 49 (W1), gkab447-. 10.1093/nar/gkab447.

(37). Babicki S; Arndt D; Marcu A; Liang Y; Grant JR; Maciejewski A; Wishart DS Heatmapper: Web-Enabled Heat Mapping for All. Nucleic Acids Res. 2016, 44 (W1), W147–W153. 10.1093/nar/gkw419. [PubMed: 27190236]

(38). Deutsch EW; Csordas A; Sun Z; Jarnuczak A; Perez-Riverol Y; Ternent T; Campbell DS; Bernal-Llinares M; Okuda S; Kawano S; Moritz RL; Carver JJ; Wang M; Ishihama Y; Bandeira N; Hermjakob H; Vizcaíno JA The ProteomeXchange Consortium in 2017: Supporting the Cultural Change in Proteomics Public Data Deposition. Nucleic Acids Res. 2017, 45 (D1), D1100–D1106. 10.1093/nar/gkw936. [PubMed: 27924013]

(39). Perez-Riverol Y; Bai J; Bandla C; García-Seisdedos D; Hewapathirana S; Kamatchinathan S; Kundu DJ; Prakash A; Frericks-Zipper A; Eisenacher M; Walzer M; Wang S; Brazma A; Vizcaíno JA The PRIDE Database Resources in 2022: A Hub for Mass Spectrometry-Based Proteomics Evidences. Nucleic Acids Res. 2021, 50 (D1), D543–D552. 10.1093/nar/gkab1038.

(40). Boudreau É; Labib S; Bertrand AT; Decostre V; Bolongo PM; Sylvius N; Bonne G; Tesson F Lamin A/C Mutants Disturb Sumo1 Localization and Sumoylation in Vitro and in Vivo. PLoS ONE 2012, 7 (9), e45918. 10.1371/journal.pone.0045918. [PubMed: 23029315]

(41). Aballo TJ; Roberts DS; Melby JA; Buck KM; Brown KA; Ge Y Ultrafast and Reproducible Proteomics from Small Amounts of Heart Tissue Enabled by Azo and TimsTOF Pro. J. Proteome Res. 2021, 20 (8), 4203–4211. 10.1021/acs.jproteome.1c00446. [PubMed: 34236868]

(42). Meier F; Park MA; Mann M Trapped Ion Mobility Spectrometry and Parallel Accumulation–Serial Fragmentation in Proteomics. Mol. Cell. Proteom. 2021, 20, 100138. 10.1016/j.mcpro.2021.100138.

(43). Gueneau L; Bertrand AT; Jais J-P; Salih MA; Stojkovic T; Wehnert M; Hoeltzenbein M; Spuler S; Saitoh S; Verschueren A; Tranchant C; Beuvin M; Lacene E; Romero NB; Heath S; Zelenika D; Voit T; Eymard B; Yaou RB; Bonne G Mutations of the FHL1 Gene Cause Emery-Dreifuss Muscular Dystrophy. Am. J. Hum. Genet. 2009, 85 (3), 338–353. 10.1016/j.ajhg.2009.07.015. [PubMed: 19716112]

(44). Friedrich FW; Wilding BR; Reischmann S; Crocini C; Lang P; Charron P; Müller OJ; McGrath MJ; Vollert I; Hansen A; Linke WA; Hengstenberg C; Bonne G; Morner S; Wichter T; Madeira H; Arbustini E; Eschenhagen T; Mitchell CA; Isnard R; Carrier L Evidence for FHL1 as a Novel Disease Gene for Isolated Hypertrophic Cardiomyopathy. Hum. Mol. Genet. 2012, 21 (14), 3237–3254. 10.1093/hmg/dds157. [PubMed: 22523091]

(45). Xu L; Humphries F; Delagic N; Wang B; Holland A; Edgar KS; Hombrebueno JR; Stolz DB; Oleszycka E; Rodgers AM; Glezeva N; McDonald K; Watson CJ; Ledwidge MT; Ingram RJ; Grieve DJ; Moynagh PN ECSIT Is a Critical Limiting Factor for Cardiac Function. JCI Insight 2021, 6 (12), e142801. 10.1172/jci.insight.142801. [PubMed: 34032637]

(46). Zhao J; Yin M; Deng H; Jin FQ; Xu S; Lu Y; Mastrangelo MA; Luo H; Jin ZG Cardiac Gab1 Deletion Leads to Dilated Cardiomyopathy Associated with Mitochondrial Damage and Cardiomyocyte Apoptosis. Cell Death Differ. 2016, 23 (4), 695–706. 10.1038/cdd.2015.143. [PubMed: 26517531]

(47). Koopmann TT; Jamshidi Y; Naghibi-Sistani M; Klift H. M. van der; Birjandi H; Al-Hassnan Z; Alwadai A; Zifarelli G; Karimiani EG; Sedighzadeh S; Bahreini A; Nouri N; Peter M; Watanabe K; Duyvenvoorde H. A. van; Ruivenkamp CAL; Teunissen AKK; Harkel ADJT; Duinen S. G. van; Haak MC; Prada CE; Santen GWE; Maroofian R. Biallelic Loss of LDB3 Leads to a Lethal Pediatric Dilated Cardiomyopathy. Eur. J. Hum. Genet. 2023, 31 (1), 97–104. 10.1038/s41431-022-01204-9. [PubMed: 36253531]

(48). Martínez-Morentin L; Martínez L; Piloto S; Yang H; Schon EA; Garesse R; Bodmer R; Ocorr K; Cervera M; Arredondo JJ Cardiac Deficiency of Single Cytochrome Oxidase Assembly Factor

Scox Induces P53-Dependent Apoptosis in a Drosophila Cardiomyopathy Model. Hum. Mol. Genet. 2015, 24 (13), 3608–3622. 10.1093/hmg/ddv106. [PubMed: 25792727]

(49). Manford AG; Rodríguez-Pérez F; Shih KY; Shi Z; Berdan CA; Choe M; Titov DV; Nomura DK; Rape M A Cellular Mechanism to Detect and Alleviate Reductive Stress. Cell 2020, 183 (1), 46–61.e21. 10.1016/j.cell.2020.08.034. [PubMed: 32941802]

(50). Choi JC; Muchir A; Wu W; Iwata S; Homma S; Morrow JP; Worman HJ Temsirolimus Activates Autophagy and Ameliorates Cardiomyopathy Caused by Lamin A/C Gene Mutation. Sci. Transl. Med. 2012, 4 (144), 144ra102. 10.1126/scitranslmed.3003875.

(51). Fatkin D; MacRae C; Sasaki T; Wolff MR; Porcu M; Frenneaux M; Atherton J; Vidaillet HJ; Spudich S; Girolami UD; Seidman JG; Muntoni F; Müehle G; Johnson W; McDonough B; Seidman CE Missense Mutations in the Rod Domain of the Lamin A/C Gene as Causes of Dilated Cardiomyopathy and Conduction-System Disease. New Engl J Med 1999, 341 (23), 1715–1724. 10.1056/nejm199912023412302. [PubMed: 10580070]

(52). Ma J; Guo L; Fiene SJ; Anson BD; Thomson JA; Kamp TJ; Kolaja KL; Swanson BJ; January CT High Purity Human-Induced Pluripotent Stem Cell-Derived Cardiomyocytes: Electrophysiological Properties of Action Potentials and Ionic Currents. Am. J. Physiol.-Hear. Circ. Physiol. 2011, 301 (5), H2006–H2017. 10.1152/ajpheart.00694.2011.

(53). Napiwocki BN; Stempien A; Lang D; Kruepke RA; Kim G; Zhang J; Eckhardt LL; Glukhov AV; Kamp TJ; Crone WC Micropattern Platform Promotes Extracellular Matrix Remodeling by Human PSC-derived Cardiac Fibroblasts and Enhances Contractility of Co-cultured Cardiomyocytes. Physiol. Rep. 2021, 9 (19), e15045. 10.14814/phy2.15045. [PubMed: 34617673]

(54). Earle AJ; Kirby TJ; Fedorchak GR; Isermann P; Patel J; Iruvanti S; Moore SA; Bonne G; Wallrath LL; Lammerding J Mutant Lamins Cause Nuclear Envelope Rupture and DNA Damage in Skeletal Muscle Cells. Nat. Mater. 2020, 19 (4), 464–473. 10.1038/s41563-019-0563-5. [PubMed: 31844279]

(55). Sun Y; Chen C; Xue R; Wang Y; Dong B; Li J; Chen C; Jiang J; Fan W; Liang Z; Huang H; Fang R; Dai G; Yan Y; Yang T; Li X; Huang Z-P; Dong Y; Liu C Maf1 Ameliorates Cardiac Hypertrophy by Inhibiting RNA Polymerase III through ERK1/2. Theranostics 2019, 9 (24), 7268–7281. 10.7150/thno.33006. [PubMed: 31695767]

(56). Muchir A; Shan J; Bonne G; Lehnart SE; Worman HJ Inhibition of Extracellular Signal-Regulated Kinase Signaling to Prevent Cardiomyopathy Caused by Mutation in the Gene Encoding A-Type Lamins. Hum. Mol. Genet. 2009, 18 (2), 241–247. 10.1093/hmg/ddn343. [PubMed: 18927124]

(57). Santini GT; Shah PP; Karnay A; Jain R Aberrant Chromatin Organization at the Nexus of Laminopathy Disease Pathways. Nucleus 2022, 13 (1), 302–314. 10.1080/19491034.2022.2153564.

(58). Luan Y; Tang N; Yang J; Liu S; Cheng C; Wang Y; Chen C; Guo Y; Wang H; Zhao W; Zhao Q; Li W; Xiang M; Ju R; Xie Z Deficiency of Ribosomal Proteins Reshapes the Transcriptional and Translational Landscape in Human Cells. Nucleic Acids Res. 2022, 50 (12), gkac053-. 10.1093/nar/gkac053.

(59). Shah PP; Lv W; Rhoades JH; Poleshko A; Abbey D; Caporizzo MA; Linares-Saldana R; Heffler JG; Sayed N; Thomas D; Wang Q; Stanton LJ; Bedi K; Morley MP; Cappola TP; Owens AT; Margulies KB; Frank DB; Wu JC; Rader DJ; Yang W; Prosser BL; Musunuru K; Jain R Pathogenic LMNA Variants Disrupt Cardiac Lamina-Chromatin Interactions and de-Repress Alternative Fate Genes. Cell Stem Cell 2021, 28 (5), 938–954.e9. 10.1016/j.stem.2020.12.016. [PubMed: 33529599]

(60). Casad ME; Abraham D; Kim I-M; Frangakis S; Dong B; Lin N; Wolf MJ; Rockman HA Cardiomyopathy Is Associated with Ribosomal Protein Gene Haplo-Insufficiency in Drosophila Melanogaster. Genetics 2011, 189 (3), 861–870. 10.1534/genetics.111.131482. [PubMed: 21890737]

(61). Zhang Y-Q; Sarge KD Sumoylation Regulates Lamin A Function and Is Lost in Lamin A Mutants Associated with Familial Cardiomyopathies. J. Cell Biol. 2008, 182 (1), 35–39. 10.1083/jcb.200712124. [PubMed: 18606848]

(62). Carmosino M; Gerbino A; Schena G; Procino G; Miglionico R; Forleo C; Favale S; Svelto M The Expression of Lamin A Mutant R321X Leads to Endoplasmic Reticulum Stress with Aberrant Ca2+ Handling. J. Cell. Mol. Med. 2016, 20 (11), 2194–2207. 10.1111/jcmm.12926. [PubMed: 27421120]

(63). Yang J; Argenziano MA; Angulo MB; Bertalovitz A; Beidokhti MN; McDonald TV Phenotypic Variability in IPSC-Induced Cardiomyocytes and Cardiac Fibroblasts Carrying Diverse LMNA Mutations. Front. Physiol. 2021, 12, 778982. 10.3389/fphys.2021.778982. [PubMed: 34975533]

(64). Maynard S; Hall A; Galanos P; Rizza S; Yamamoto T; Gram HH; Munk SHN; Shoaib M; Sørensen CS; Bohr VA; Lerdrup M; Maya-Mendoza A; Bartek J Lamin A/C Impairments Cause Mitochondrial Dysfunction by Attenuating PGC1α and the NAMPT-NAD+ Pathway. Nucleic Acids Res. 2022, 50 (17), 9948–9965. 10.1093/nar/gkac741. [PubMed: 36099415]

(65). Sieprath T; Darwiche R; Vos WHD Lamins as Mediators of Oxidative Stress. Biochem. Biophys. Res. Commun. 2012, 421 (4), 635–639. 10.1016/j.bbrc.2012.04.058. [PubMed: 22538370]

(66). Rodriguez BM; Domínguez-Rodríguez A; Benitah J-P; Lefebvre F; Marais T; Mougenot N; Beauverger P; Bonne G; Briand V; Gómez A-M; Muchir A Activation of Sarcolipin Expression and Altered Calcium Cycling in LMNA Cardiomyopathy. Biochem. Biophys. Rep. 2020, 22, 100767. 10.1016/j.bbrep.2020.100767. [PubMed: 32490213]

(67). Narasimhan M; Rajasekaran NS Reductive Potential — A Savior Turns Stressor in Protein Aggregation Cardiomyopathy. Biochim. Biophys. Acta (BBA) - Mol. Basis Dis. 2015, 1852 (1), 53–60. 10.1016/j.bbadis.2014.11.010.

(68). Romuk E; Jacheć W; Kozielska-Nowalany E; Birkner E; Zemła-Woszek A; Wojciechowska C Superoxide Dismutase Activity as a Predictor of Adverse Outcomes in Patients with Nonischemic Dilated Cardiomyopathy. Cell Stress Chaperones 2019, 24 (3), 661–673. 10.1007/s12192-019-00991-3. [PubMed: 31041645]

(69). Voos W; Pollecker K The Mitochondrial Lon Protease: Novel Functions off the Beaten Track? Biomolecules 2020, 10 (2), 253. 10.3390/biom10020253. [PubMed: 32046155]

(70). Jeong S-J; Park J-G; Oh GT Peroxiredoxins as Potential Targets for Cardiovascular Disease. Antioxidants 2021, 10 (8), 1244. 10.3390/antiox10081244. [PubMed: 34439492]

(71). Fan Y; Tan D; Zhang X; Song D; Chang X; Wang S; Yan H; Ge L; Yang H; Bönnemann C; Liu J; Wang S; Wu X; Zhang H; Xiong H Nuclear Factor-KB Pathway Mediates the Molecular Pathogenesis of LMNA-Related Muscular Dystrophies. Biochem. Genet. 2020, 58 (6), 966–980. 10.1007/s10528-020-09989-4. [PubMed: 32705401]

(72). Lammerding J; Schulze PC; Takahashi T; Kozlov S; Sullivan T; Kamm RD; Stewart CL; Lee RT Lamin A/C Deficiency Causes Defective Nuclear Mechanics and Mechanotransduction. J. Clin. Investig. 2004, 113 (3), 370–378. 10.1172/jci19670. [PubMed: 14755334]

(73). Muchir A; Wu W; Choi JC; Iwata S; Morrow J; Homma S; Worman HJ Abnormal P38α Mitogen-Activated Protein Kinase Signaling in Dilated Cardiomyopathy Caused by Lamin A/C Gene Mutation. Hum. Mol. Genet. 2012, 21 (19), 4325–4333. 10.1093/hmg/dds265. [PubMed: 22773734]

(74). Chen SN; Lombardi R; Karmouch J; Tsai J-Y; Czernuszewicz G; Taylor MRG; Mestroni L; Coarfa C; Gurha P; Marian AJ DNA Damage Response/TP53 Pathway Is Activated and Contributes to the Pathogenesis of Dilated Cardiomyopathy Associated With LMNA (Lamin A/C) Mutations. Circ. Res. 2019, 124 (6), 856–873. 10.1161/circresaha.118.314238. [PubMed: 30696354]

(75). Osorio FG; Bárcena C; Soria-Valles C; Ramsay AJ; Carlos F. de; Cobo J; Fueyo A; Freije JMP; López-Otín C. Nuclear Lamina Defects Cause ATM-Dependent NF-KB Activation and Link Accelerated Aging to a Systemic Inflammatory Response. Genes Dev. 2012, 26 (20), 2311–2324. 10.1101/gad.197954.112. [PubMed: 23019125]

(76). Chandran S; Suggs JA; Wang BJ; Han A; Bhide S; Cryderman DE; Moore SA; Bernstein SI; Wallrath LL; Melkani GC Suppression of Myopathic Lamin Mutations by Muscle-Specific Activation of AMPK and Modulation of Downstream Signaling. Hum. Mol. Genet. 2018, 28 (3), 351–371. 10.1093/hmg/ddy332.

(77). Pande S; Ghosh DK Nuclear Proteostasis Imbalance in Laminopathy-associated Premature Aging Diseases. FASEB J. 2023, 37 (8), e23116. 10.1096/fj.202300878r. [PubMed: 37498235]

(78). Wang C; Wang X The Interplay between Autophagy and the Ubiquitin–Proteasome System in Cardiac Proteotoxicity. Biochim. Biophys. Acta (BBA) - Mol. Basis Dis. 2015, 1852 (2), 188–194. 10.1016/j.bbadis.2014.07.028.

(79). Wong DCP; Xiao J; Chew TW; Pan M; Lee CJM; Ang JW; Yow I; Thivakar T; Ackers-Johnson M; Lee NJW; Foo RS; Kanchanawong P; Low BC BNIP-2 Activation of Cellular Contractility Inactivates YAP for H9c2 Cardiomyoblast Differentiation. Adv. Sci. 2022, 9 (31), 2202834. 10.1002/advs.202202834.

(80). Korfali N; Wilkie GS; Swanson SK; Srsen V; Heras J. de las; Batrakou DG; Malik P; Zuleger N; Kerr ARW; Florens L; Schirmer EC. The Nuclear Envelope Proteome Differs Notably between Tissues. Nucleus 2012, 3 (6), 552–564. 10.4161/nucl.22257. [PubMed: 22990521]

(81). Marks AR Calcium Cycling Proteins and Heart Failure: Mechanisms and Therapeutics. J. Clin. Investig. 2013, 123 (1), 46–52. 10.1172/jci62834. [PubMed: 23281409]

(82). Lokuta AJ; Maertz NA; Meethal SV; Potter KT; Kamp TJ; Valdivia HH; Haworth RA Increased Nitration of Sarcoplasmic Reticulum Ca2+-ATPase in Human Heart Failure. Circulation 2005, 111 (8), 988–995. 10.1161/01.cir.0000156461.81529.d7. [PubMed: 15710754]

(83). Dridi H; Wu W; Reiken SR; Ofer RM; Liu Y; Yuan Q; Sittenfeld L; Kushner J; Muchir A; Worman HJ; Marks AR Ryanodine Receptor Remodeling in Cardiomyopathy and Muscular Dystrophy Caused by Lamin A/C Gene Mutation. Hum. Mol. Genet. 2021, 29 (24), 3919–3934. 10.1093/hmg/ddaa278. [PubMed: 33388782]

(84). Choi B-R; Liu T; Salama G Calcium Transients Modulate Action Potential Repolarizations in Ventricular Fibrillation. 2006 Int. Conf. IEEE Eng. Med. Biol. Soc. 2006, 2006, 2264–2267. 10.1109/iembs.2006.260059.

(85). Hamilton S; Terentyev D ER Stress and Calcium-Dependent Arrhythmias. Front. Physiol. 2022, 13, 1041940. 10.3389/fphys.2022.1041940. [PubMed: 36425292]

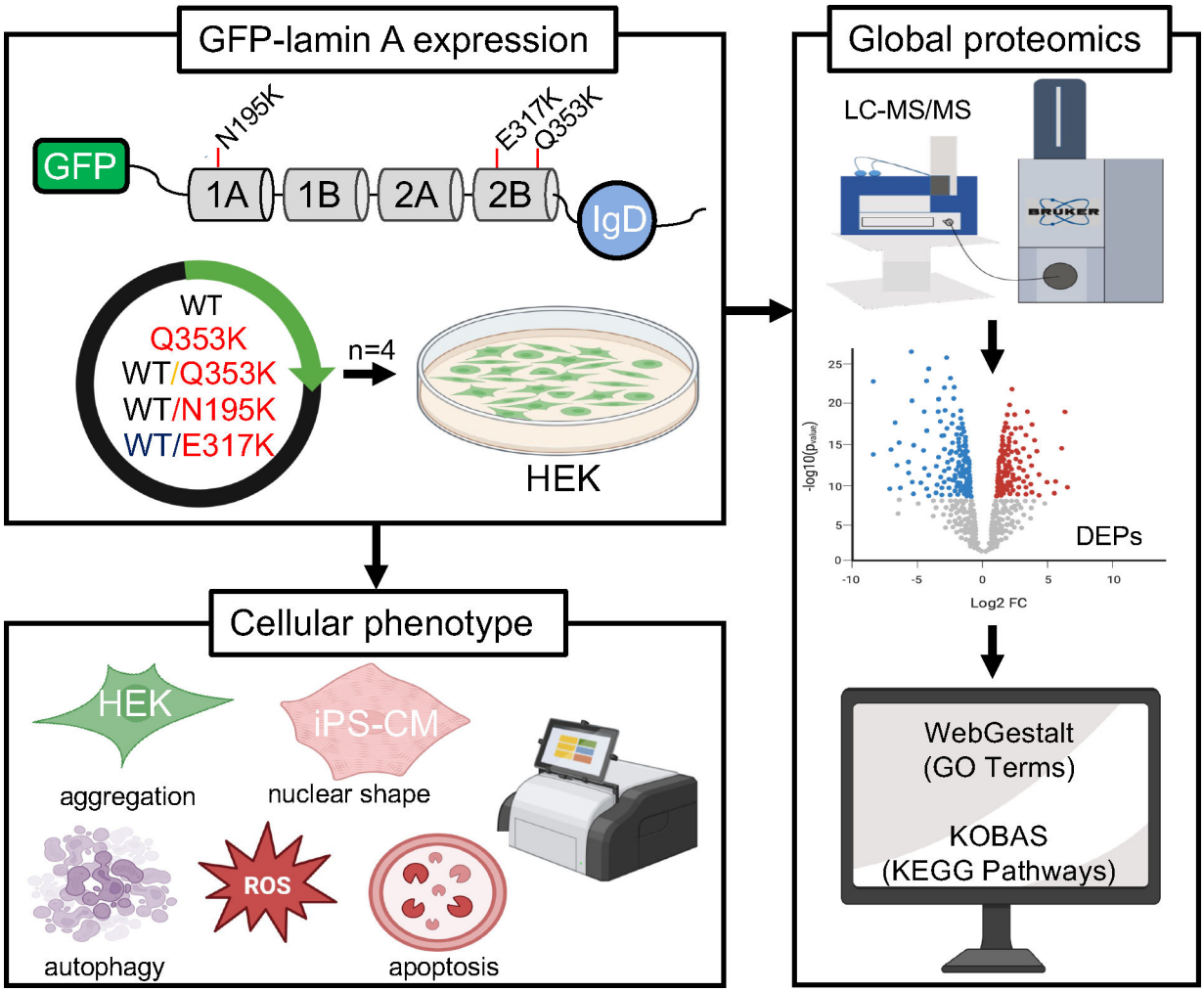

Fig. 1.

Schematic of experimental design and analysis. GFP-tagged lamin A mutants were expressed in HEK cells and imaged for aggregation, functional and mass spectrometry analyses for comparisons. CCD; Coiled coil domain, IgD; immunoglobulin-like domain, iPS-CM; induced pluripotent stem cell-derived cardiomyocytes, LC-MS/MS; liquid chromatography tandem mass spectrometry, DEP; differentially expressed proteins. Some images obtained from BioRender.com.

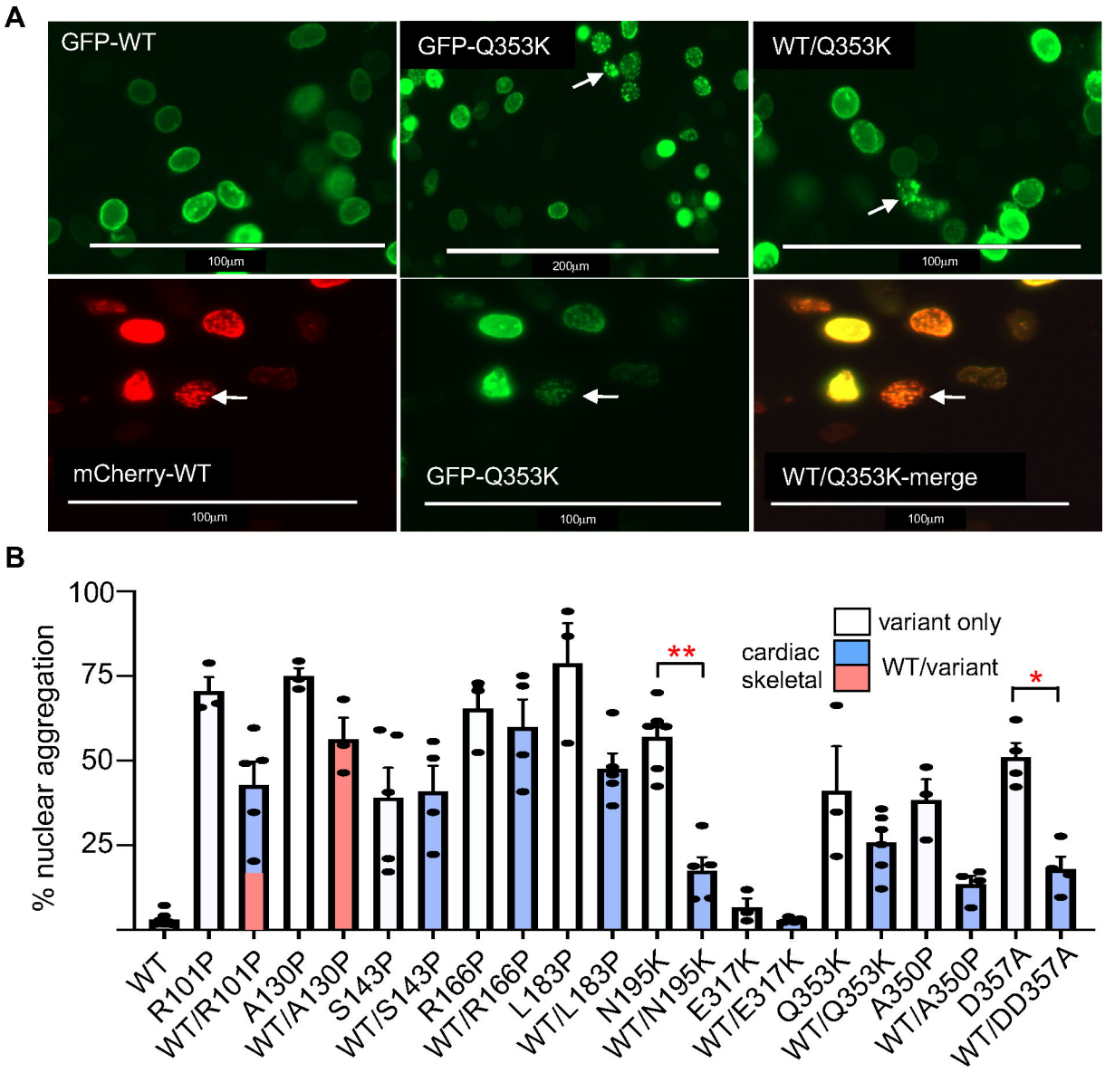

Fig. 2.

LMNA aggregation analyses. Imaging of GFP-lamin A over-expressed in (**A**) HEK 293 cells showing nuclear aggregation (arrows) for Q353K co-expressed with WT compared to WT alone. (**B**) Percentage of cells containing nuclear aggregates for mutants co-expressed with WT (color coded by clinical phenotype) compared to our previously published mutant alone data[15]. Error bars represent mean ± SEM of biological replicates. *$p < 0.05$.

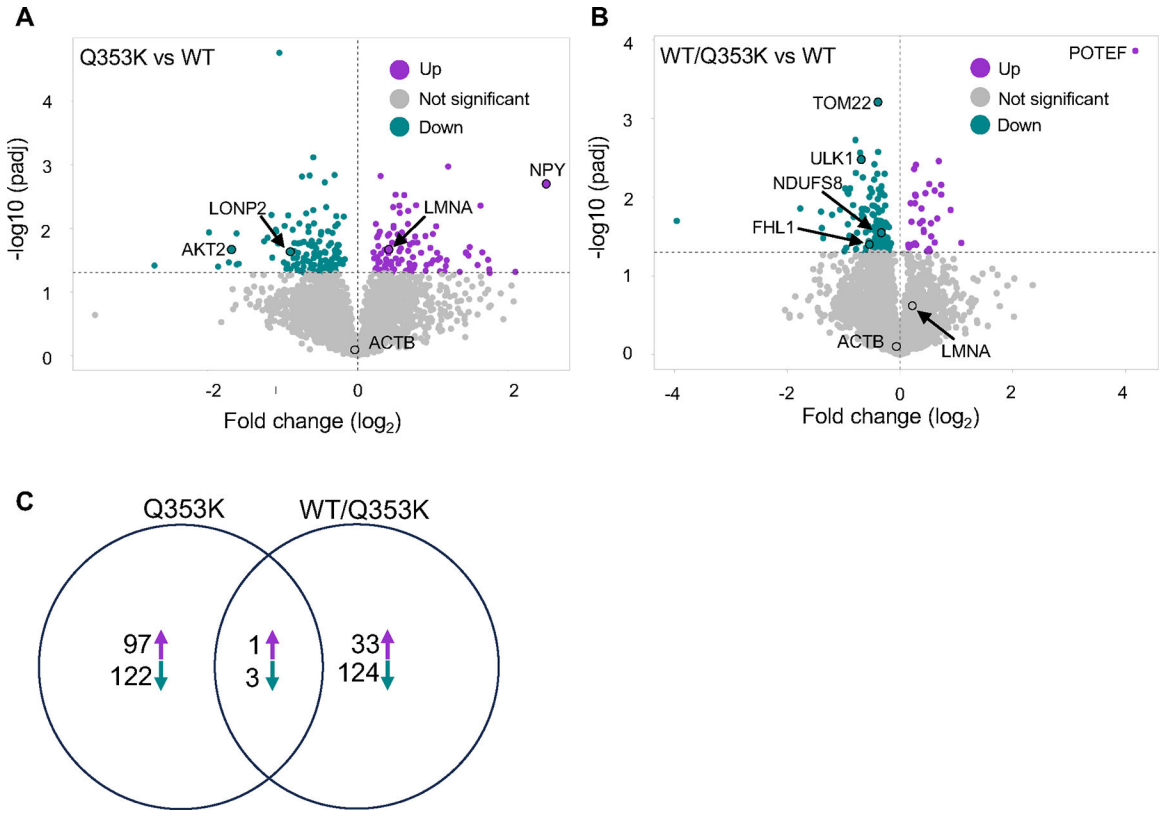

Fig. 3.

Proteomic changes comparing homomeric over-expression of Q353K lamin A and heteromeric WT/Q353K lamin A in HEK cells versus WT. Volcano plots showing all proteins identified with DEPs (padj < 0.05) in purple and green for (**A**) homomeric and (**B**) heteromeric WT/Q353K compared to WT. Examples highlighted are discussed and cited. (**C**) Venn diagram comparing DEPs from homomeric Q353K and heteromeric WT/Q353K datasets.

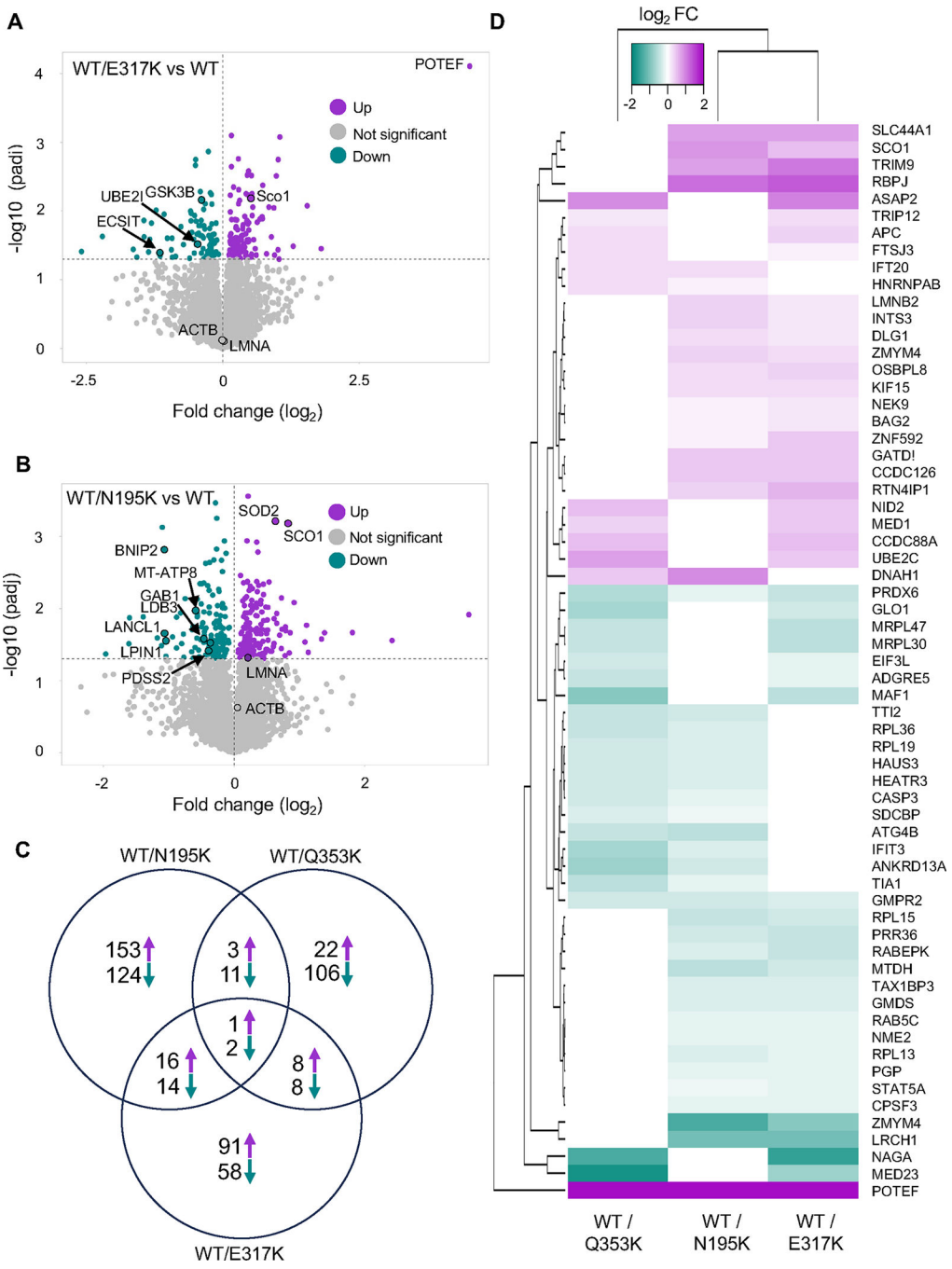

Fig. 4.

Proteomic changes comparing heteromeric over-expression of WT/Q353K, WT/E317K, and WT/N195K lamin A in HEK cells versus to WT. Volcano plots showing all proteins identified with DEPs (padj < 0.05) in purple and green for (**A**) WT/E317K and (**B**) heteromeric WT/N195K versus WT. Examples highlighted are discussed and cited. (**C**) Venn diagram comparing DEPs from the three heteromeric datasets. (**D**) Heatmap of the overlapping DEPs. The outlier POTEF's values were capped at two to reduce washout.

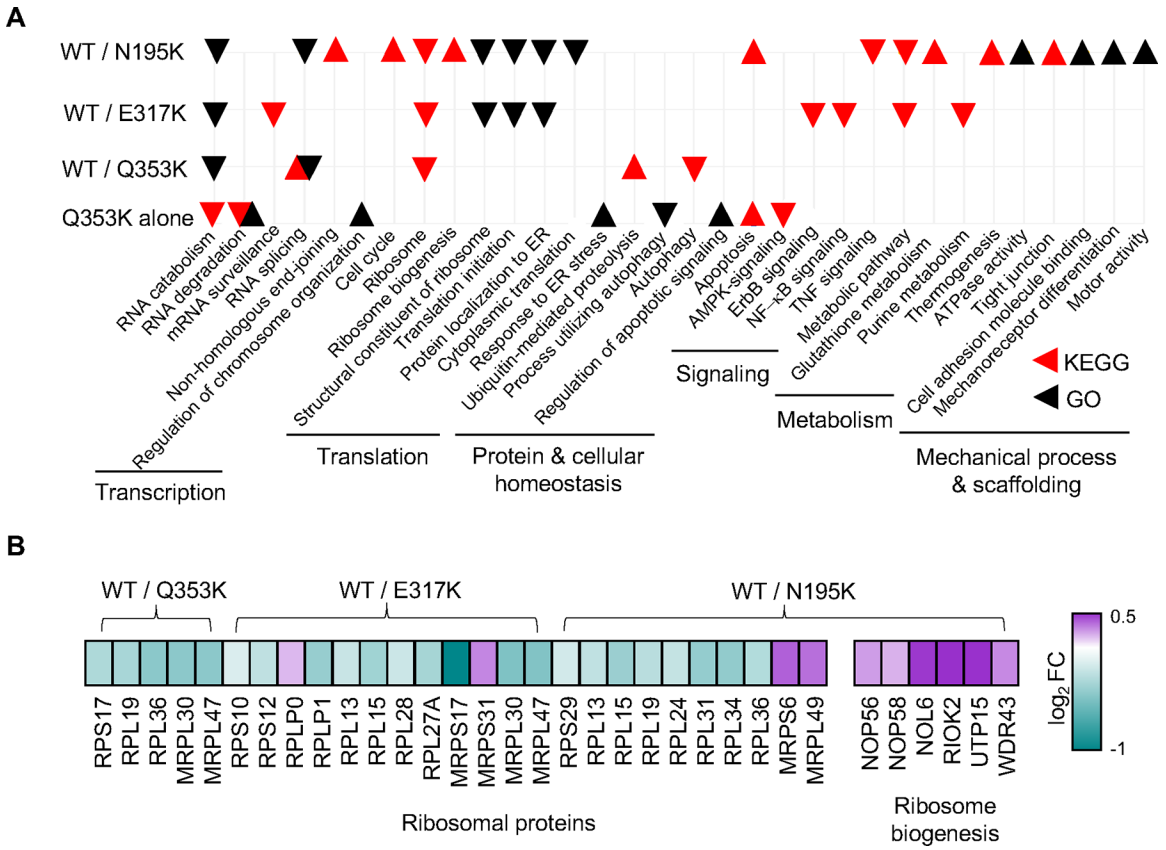

Fig. 5.

Summary of GO Term and KEGG analyses. (**A**) GO Terms (black) and KEGG pathways (red) associated with up-regulated (up arrow) and down-regulated (down arrow) proteins from each proteomic dataset are categorized into six similar groups. (**B**) All DEPs involved in ribosomal function and highlighted for each dataset.

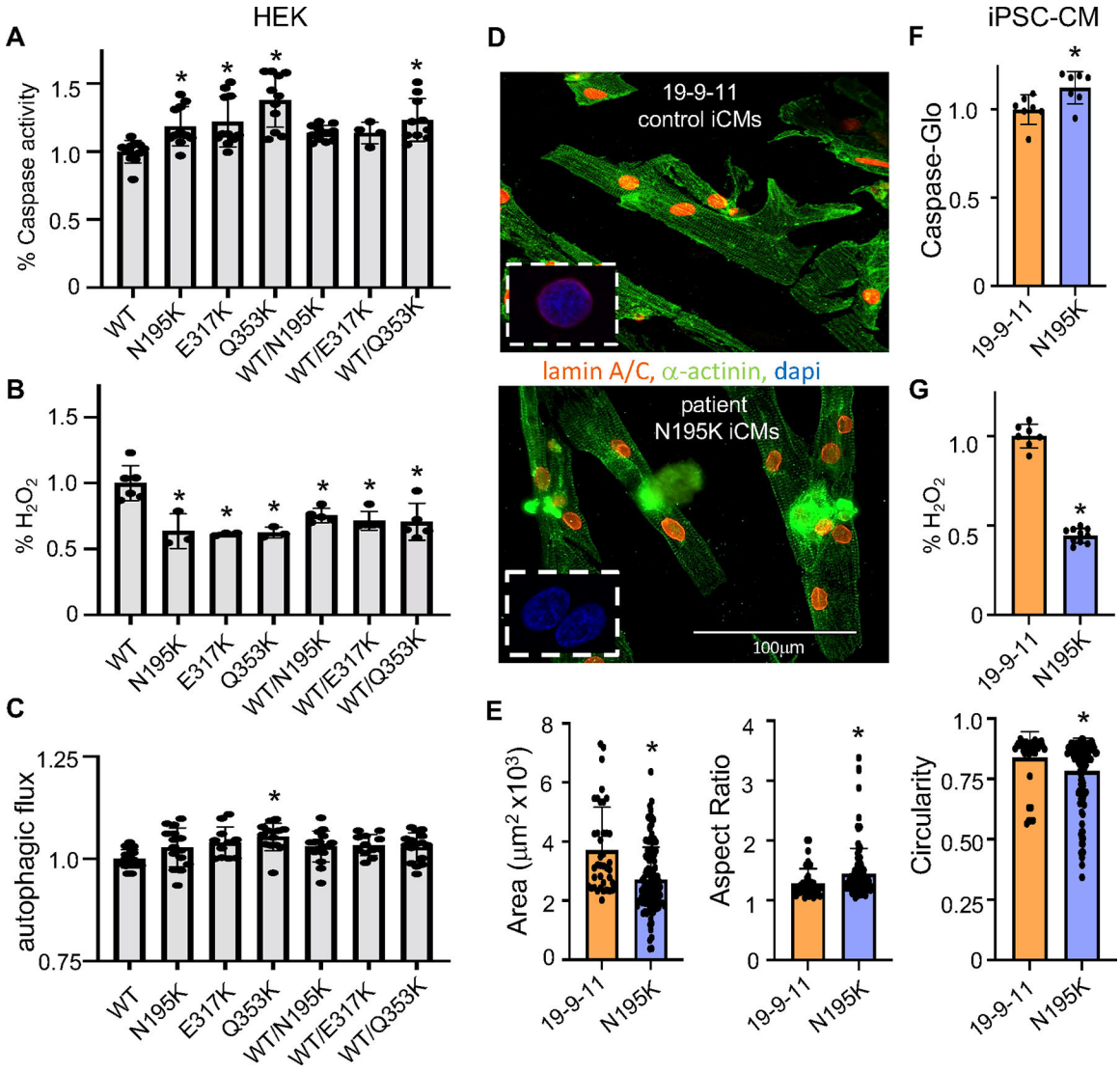

Fig. 6.

Functional analysis of laminopathic mutations. (**A**) Caspase 3/7 activity in HEK 293 cells as a measure of apoptosis. (**B**) Hydrogen peroxide levels in HEK 293 cells as a measure of redox state. (**C**) Autophagic flux levels (inversely proportional to flux) in HEK 293 cells. (**D**) Lamin A/C and α-actinin staining of iPSC-CMs from control 19-9-11 and patient N195K iPSC-CMs. Inset shows DAPI staining examples used for the three nuclear shape measurements in (**E**). (**F**) Caspase 3/7 activity in iPSC-CMs. (**G**) Hydrogen peroxide levels in iPSC-CMs. Error bars are mean ± sd of biological replicates (*p < 0.05).